Atmospheric Chemistry Experiment (ACE) observations of aerosol in the upper troposphere and lower stratosphere from the Kasatochi volcanic eruption

C. E. Sioris,[1,2] C. D. Boone,[3] P. F. Bernath,[3,4] J. Zou,[5] C. T. McElroy,[1] and C. A. McLinden[1]

Received 30 November 2009; revised 29 June 2010; accepted 7 July 2010; published 27 October 2010.

[1] Near-infrared (NIR) atmospheric extinction profile observations from the Atmospheric Chemistry Experiment (ACE) Imager and from Measurements of Aerosol Extinction in the Stratosphere and Troposphere Retrieved by Occultation (MAESTRO) are presented, illustrating the impact of the Kasatochi volcanic eruption in August 2008 on the aerosol loading of the upper troposphere and lower stratosphere in the subsequent months. In September 2008, profiles of NIR extinction show a significant increase relative to each of the previous four Septembers (2004–2007). The aerosol enhancement is observable up to 18.5 km in Northern Hemisphere NIR extinction data, and peaks at 9.5 km in the extratropics, where the extinction is ~8 times the normal September value. The particulate matter in the troposphere is quickly dispersed over the Northern Hemisphere during September 2008 and vanishes by the end of November 2008. An upper layer, initially in the extratropical lower stratosphere, persists through March 2009, descending with time into the troposphere where, by coagulation of sulphate aerosol, the size of the particles increases with time.

Citation: Sioris, C. E., C. D. Boone, P. F. Bernath, J. Zou, C. T. McElroy, and C. A. McLinden (2010), Atmospheric Chemistry Experiment (ACE) observations of aerosol in the upper troposphere and lower stratosphere from the Kasatochi volcanic eruption, *J. Geophys. Res.*, *115*, D00L14, doi:10.1029/2009JD013469.

1. Introduction

[2] Large volcanic eruptions can lead to changes in incoming radiation at the surface, and even a strong cooling effect on a global scale. For example, it is estimated that the large eruption of Mount Pinatubo in 1991 led to a mean decrease in lower tropospheric temperature of 0.7 K by September 1992 [*Dutton and Christy*, 1992].

[3] Kasatochi Volcano erupted explosively three times between 7 and 8 August 2008. Ash from these major explosions reached 16 km above sea level (ASL) according to CALIPSO (Cloud-Aerosol Lidar and Infrared Pathfinder Satellite Observation) observations on the following day [*Yang et al.*, 2010]. Following these eruptions, a continuous phase of ash emission continued for hours, reaching 11 km ASL (http://avo.alaska.edu/activity/Kasatochi.php). This eruption produced the greatest stratospheric abundance of SO_2 (the primary aerosol precursor) in this decade thus far [*Carn et al.*, 2008; *Yang et al.*, 2010]. A peak height of 8 to 12 km for bromine monoxide emitted by the Kasatochi eruption has been inferred from GOME-2 measurements and FLEXPART modeling [*Theys et al.*, 2009], and *Yang et al.* [2010] also found SO_2 with the same peak height (9–11 km).

[4] As part of the Atmospheric Chemistry Experiment (ACE) mission, the SCISAT satellite was launched in August 2003 [*Bernath*, 2006] bearing three instruments relying on the solar occultation technique to measure profiles of trace gases or aerosol extinction. Scientific data products from these instruments are available from February 2004 onward.

[5] The ACE Imager measures atmospheric extinction in the near-infrared (NIR) at ~1020 nm, which at altitudes above 5 km, is largely dominated by aerosol scattering, and also at ~525 nm. For the extinction retrieval, the imager data used covers an area of the detector that when projected to the tangent point is 0.7 km tall and 2.1 km wide [*Gilbert et al.*, 2007]. The optical filters were designed to match two of the SAGE II channels. The algorithm to retrieve extinctions from the NIR and visible imager data is described by *Gilbert et al.* [2007]. *Vanhellemont et al.* [2008] isolate the profile extinction owing to aerosols, compare these profiles with correlative measurements, and list some of the instrumental issues of the imagers. The NIR Imager aerosol extinctions are within a few percent of correlative measurements in the troposphere and in good agreement up to 25 km [*Vanhellemont*

[1]Environment Canada, Toronto, Ontario, Canada.
[2]Also at Harvard-Smithsonian Center for Astrophysics, Cambridge, Massachusetts, USA.
[3]Department of Chemistry, University of Waterloo, Waterloo, Ontario, Canada.
[4]Now at Department of Chemistry, University of York, York, UK.
[5]Department of Physics, University of Toronto, Toronto, Ontario, Canada.

0148-0227/10/2009JD013469

et al., 2008]. Thus, given that the current study is essentially focused on the altitude range below 25 km, the instrumental issues are of minor consequence.

[6] The MAESTRO instrument is described by *McElroy et al.* [2007]. The height and width of the MAESTRO field-of-view are 1.2 and 25 km, respectively (at a tangent height of 22 km). Finally, the primary instrument is the Fourier Transform Spectrometer (FTS), which measures profiles of temperature and a suite of chemical constituents with 4 km vertical resolution. The vertical resolution of MAESTRO and the NIR Imager is better than any other satellite-borne passive remote sensor currently capable of monitoring the evolution of a volcanic aerosol layer. Only these ACE instruments use the solar occultation technique and provide global coverage of stratospheric and upper tropospheric aerosols. The limb-viewing solar occultation technique allows for very high precision. SCIAMACHY solar occultation events are limited to high northern latitudes. GOMOS uses stellar occultation and has coarser vertical resolution [*Vanhellemont et al.*, 2005]. Another advantage of the SCISAT orbit is that the spatiotemporal sampling pattern repeats yearly, which is convenient for the analysis of temporal trends.

[7] The purpose of this paper is to show that the ACE instruments made global observations of the vertical profile of extinction during the post-Kasatochi period, monitoring the dispersion of the greatly enhanced volcanic aerosol abundance through the Northern Hemisphere. This paper also shows that two distinct aerosol layers appeared in the month following the Kasatochi volcanic eruption (i.e., September 2008): one near the midlatitude tropopause (~10 km) and a second in the lower stratosphere. A secondary objective of this paper relates to the ongoing estimation of background stratospheric aerosol levels. We illustrate that, through November 2008, the extinction in a given satellite measurement above ~10 km could be classified as perturbed or unperturbed by the Kasatochi eruption, but by December 2008, the observed Northern Hemisphere background aerosol extinction had jumped relative to the pre-Kasatochi period as the volcanic aerosols became more homogeneously distributed in space during the months following the eruption.

2. Method

[8] In this section, the method used to discriminate between clouds and background aerosol is described. This ability to discriminate between clouds (including fresh volcanic plumes) and background aerosols allows for the determination of cloud top heights and the clear-sky aerosol extinction profile from the NIR Imager observations. It also allows for three-dimensional mapping of this relatively long-lived volcanic plume. Previous work on cloud heights from ACE Imager extinctions relied on visual inspection [*Dodion et al.*, 2007]. This method was limiting since:

[9] 1. It is extremely time-consuming to analyze several years (e.g., 2004–2009) of data as is done here. This period comprises more than 20,000 profiles.

[10] 2. The magnitude of the extinction is neglected, as this technique relies simply on the shape of the extinction profile. Consequently, strong vertical gradients of background Junge layer aerosol could be misinterpreted as a cloud, even though the aerosol extinction is small. Nevertheless, the visual inspection technique serves as verification for any automated method.

[11] The method used here is based on the work of *Fromm et al.* [2003], but differs in many respects so, rather than list the differences, the algorithm used here is described in full. First, the data are separated by month. Then profiles for that month which are monotonically increasing in terms of NIR (~1020 nm) total extinction with decreasing altitude below 30 km are selected. These profiles are separated from those that do not exhibit this monotonic decrease, forming "clear" and "cloudy" subsets. The median and standard deviation (σ) of the NIR extinction at each altitude for the "clear" group are determined. Then, if the extinction at any altitude below 25 km of any individual member of this subset is greater than the group median $+4\sigma$, the layer exhibiting such a value is filtered out to compute a new median and σ at that altitude using the remaining observations. A final median and σ vertical profile is obtained iteratively (where necessary). This iterative process removes observations that are monotonic but likely affected by thick cloud in the lowest retrieval layer, called "high z_min" cases by *Fromm et al.* [2003].

[12] The monotonic profile criterion, not used by *Fromm et al.* [2003], is effective for separating cloudy from cloud-free profiles, particularly for tropospheric clouds, because condensation occurs at the lifting condensation level [*Salby*, 1996], below which the extinction tends to be sharply lower. Even for clouds which form in the absence of convection (e.g., near the tropical tropopause), condensation occurs at a level where the temperature is sufficiently low, and given the mean temperature gradient in the troposphere (i.e., steadily decreasing with altitude), layered cloud is expected, and below this vertical level of condensation/crystallization, the extinction will be smaller.

[13] This process of determining the clear-sky extinction and identifying clouds is repeated for each month. The resulting clear-sky extinction time series is displayed in Figure 1 in the 10.5–24.5 km altitude range. The time series is remarkably smooth above 18 km considering that the latitudinal sampling of ACE changes as a function of month as shown by *Bernath* [2006]. To construct a monthly time series in a latitude band is not possible because of the limited spatial sampling and measurement frequency of ACE. Certain maxima remain in the time series at the altitude of frequent polar stratospheric cloud formation in August 2004, 2006, and 2008 and in February 2007 and 2008 when the winter polar vortices were sampled. These maxima arise from high extinction in the lowest layer of the individual profiles. For these cases, ACE's sun tracker becomes ineffective immediately below this altitude because of optically thick cloud.

[14] The median and standard deviation of all profiles and of those with monotonically decreasing extinction with increasing altitude were examined (Figure 2). The medians show small relative differences, but the averages and standard deviations are significantly smaller for the monotonic subset. For the monotonic subset, the average agrees quite well with both the medians (monotonic subset and the entire ensemble), which is expected for normally distributed background extinction. However, using the entire ensemble of profiles, the average is larger than the median (indicating a positively skewed data set as expected) and the standard

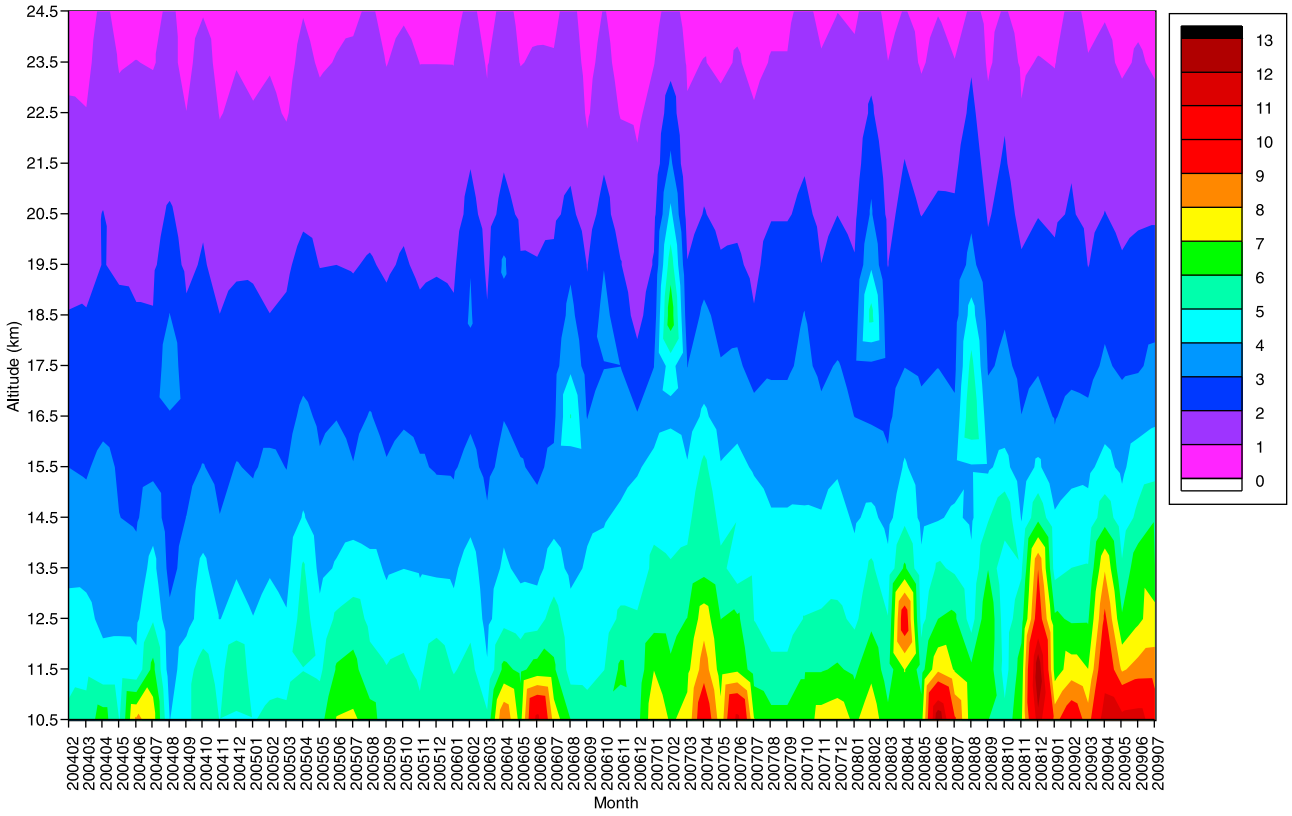

Figure 1. Cloud-cleared global median atmospheric extinction ($\times 10^{-4}$ km^{-1}) by month (YYYYMM) from the ACE NIR Imager. Note that PSCs and thin cirrus near the tropical tropopause are not perfectly filtered, leading to February and August occasionally showing a local maximum near 17.5–18.5 km.

deviation increases significantly relative to the monotonic subset, even though the sample size is much larger. There are two caveats with this method. First, it applies only to periods where no well-defined, aged Junge layer appears to exist; otherwise there would be a lack of monotonic profiles. However, since the first ACE measurement early in 2004, only the eruption at Kasatochi has perturbed stratospheric aerosol significantly to restore the Junge layer for a considerable period (>1 month). Second, the method requires very precise extinction measurements, such as those from ACE Imager. The MAESTRO aerosol extinction data retrieved for this paper, are not yet as precise, and thus measurement noise causes there to be few, if any, profiles that are monotonic below 30 km in the period of one month. Ironically, by including only monotonic profiles, noisy ACE Imager profiles are eliminated and the standard deviation of measured extinction is reduced. Thus, the advantage of limiting the data to monotonic profiles is that the standard deviation is greatly reduced, without changing the median, thus enabling a more powerful statistical detection of positive extinction outliers (i.e., clouds).

[15] Using MAESTRO optical depth spectra (version 1.2), aerosol extinction can be retrieved at several wavelengths. Here, MAESTRO aerosol extinction vertical profiles are measured at two wavelengths with minimal trace gas absorption, namely 779 and 1000 nm, with the aerosol extinction at the latter wavelength being comparable with NIR Imager atmospheric extinction. The version 1.2 data cuts off at 9 km whereas future versions will extend down to 5 km. The MAESTRO aerosol extinction retrieval uses the VECTOR forward model and its database of model atmospheres [*McLinden et al.*, 2006, and references therein]. The key atmospheric parameters are pressure, ozone, and temperature, as the temperature dependence of ozone absorption is taken into account (v3.0 O_3 cross sections at 203, 243 and 273 K; see *Bogumil et al.* [2003]). The *Chahine* [1970] relaxation technique is used to update the aerosol extinction profile during the iterative inversion, in order to match modeled and measured line-of-sight optical depths on the tangent height grid of the measurements. Within the retrieval range, the aerosol extinction profile is forward modeled on an altitude grid corresponding to the tangent height grid of the measurements. Above the retrieval range, ozone and Rayleigh extinction are simulated on a 2 km grid and aerosol extinction is assumed to be nil. The convergence criterion is determined by the noise level of the observations, and is given by the sample standard deviation (σ) of the optical depth of the five pixels whose wavelength is closest to 779 or 1000 nm. To reduce noise, the average optical depth from these same five pixels is used as the observable. The upper altitude limit of each retrieved profile is determined by the highest tangent height without a negative optical depth in the 777.91–779.90 and 972.8–1000.7 nm ranges for 779 and 1000 nm, respectively. The lower altitude is generally determined by the top height of opaque tropospheric clouds. The precision profile is calculated by numerical perturbation analysis, propagating σ of the optical depth through the retrieval. Using MAESTRO aerosol

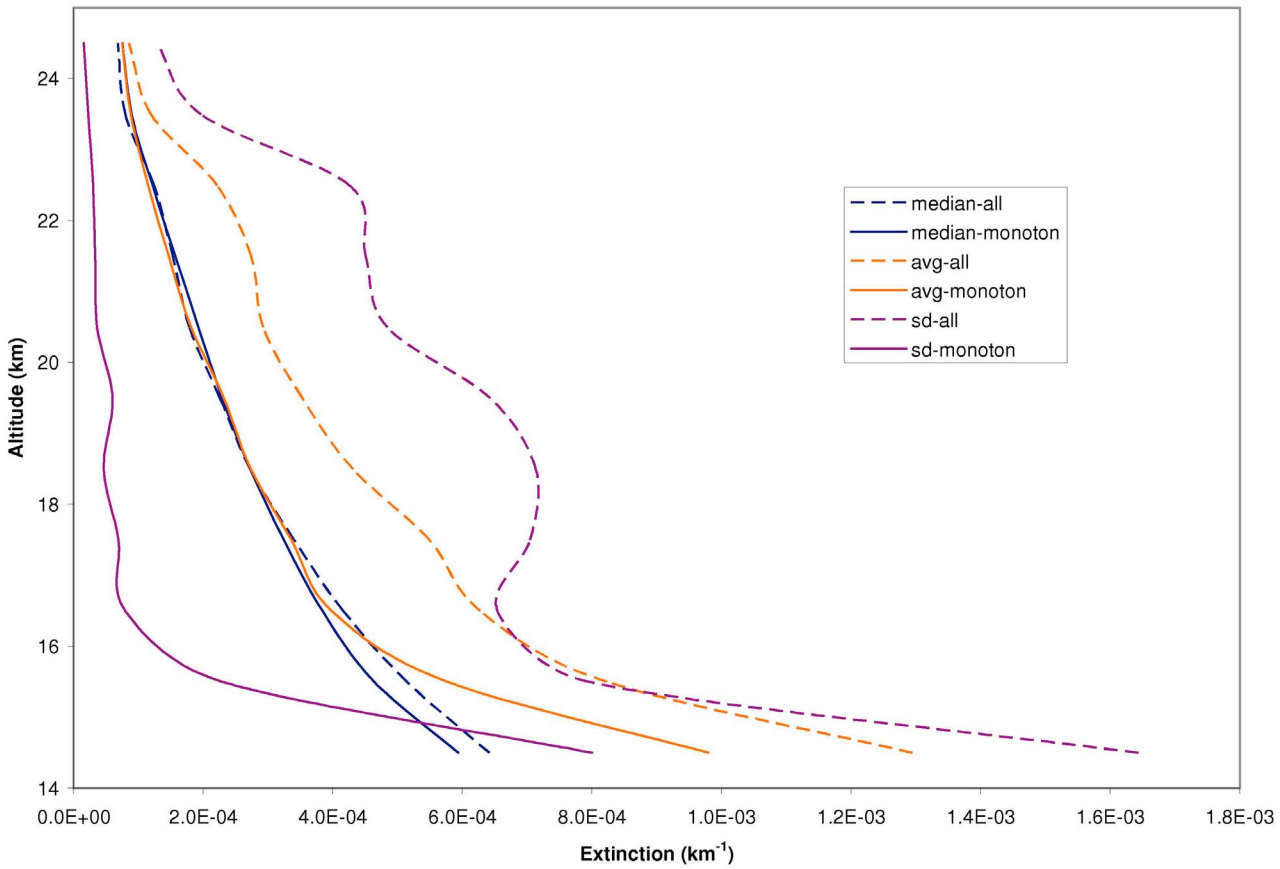

Figure 2. Statistics derived from NIR Imager extinction profiles for a random month (July 2009). The average (avg), median, and standard deviation (sd) for the entire global ensemble of profiles (all) and for the subset with monotonically (monoton) increasing extinction with decreasing altitude.

extinction measurements at two wavelengths (779 and 1000 nm) and finding the median vertical profile for all Northern Hemisphere (NH) data at each wavelength, an Ångström exponent vertical profile was derived for each month.

3. Results and Discussion

3.1. Aerosol Extinction Level Preceding the Kasatochi Eruption

[16] Owing to the limited spatial sampling of Northern Hemisphere middle and high latitudes by ACE, plumes from Kasatochi Volcano were not encountered in August 2008. However, the Okmok eruption on 12 July 2008 sent ash and gases to an altitude of 16 km [*Larsen et al.*, 2009] and is discussed here because it is relevant to the pre-Kasatochi level of aerosol extinction. Following the Okmok eruption, daily maps of sulphur dioxide from satellites indicate an eastward transport of this volcanic gas [e.g., *Rix et al.*, 2009]. NH monthly median and average NIR Imager extinction in July 2008 is almost identical to July 2006. However, for altitudes above 14.0 km, if ACE NIR Imager data is limited to latitudes >40°N to eliminate tropical high clouds, there are only three cloud detections in July 2008 with extinction greater than 10^{-3} km^{-1}. Two of these preceded the Okmok eruption, but the third cloud was observed on 27 July 2008 at 52.3°N, 83.7°W over northern Ontario, east of Okmok. NIR Imager and MAESTRO (779 and 1000 nm) observations show an extinction peak at 14.5 and 14.57 km, respectively. The 1 μm extinction observed by these two instruments at this peak is 1.05 and 1.46 × 10^{-3}, respectively, much smaller than in individual Kasatochi plume observations shown below. At 14.57 km, MAESTRO observed an Ångström exponent local maximum of 1.38, indicative of small aerosols, and not indicative of cirrus. NH median and average extinction profiles from NIR Imager are essentially monotonically increasing toward the surface in August 2008. Also, the NH median in August 2008 is not significantly larger than the mean of the monthly NH medians of previous Augusts during the ACE mission (2004, 2005, 2006). NH data is not available in August 2007. In summary, ACE observations suggest the impact of the Okmok eruption on the NH extinction in the upper troposphere and lower stratosphere was slight.

3.2. Cloud Detections and Estimation of Background Aerosol Level Following the Kasatochi Eruption

[17] Evidence of high aerosol extinction in the lower stratosphere following the Kasatochi volcanic eruption first appeared in September 2008 ACE data, when clouds were detected above 14 km in northern middle and high latitudes (34–85°N) by the NIR Imager (Figure 3). In the four previous

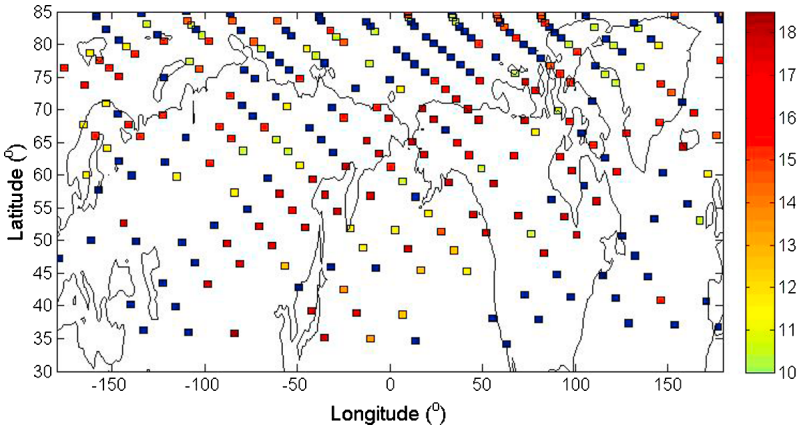

Figure 3. Map of September 2008 occultation locations (N = 549) in the Northern Hemisphere by ACE. Observations without enhanced aerosol are shown as dark blue (N = 390). The color scale indicates the highest altitude (km) at which an aerosol enhancement was detected in a given occultation (N = 159) using the cloud-finding technique described in section 2. Note that in the four previous Septembers, not a single cloud was observed above 14 km.

Septembers (2004–2007), not a single cloud above 14 km was observed by the ACE NIR Imager in this latitude range.

[18] In contrast to September 2008, by December 2008, even though the effects of the volcanic eruption have not disappeared (as shown below), sharp layers in the NIR Imager data are not readily found. Consequently, this raises estimates of background extinction for this month (Figure 1). Including data from both hemispheres, the clear-sky 1020 nm vertical optical depth between 11 and 14 km from NIR Imager for December 2008 is 3.2×10^{-3}, almost seven standard deviations above the climatological monthly average value of $(1.5 \pm 0.3) \times 10^{-3}$ (February 2004 to November 2008) and is clearly unprecedented for any month during the ACE mission. However, atmospheric extinction in the Southern Hemisphere is not noticeably affected by the Kasatochi eruption through March 2009 (not shown) and has a median profile similar to the background profiles shown in Figure 4. Thus, the relative aerosol perturbation in the Northern Hemisphere is even larger. By January 2009, the background aerosol extinction levels have returned close to normal above 10 km (see Figure 1). In April 2009, the background aerosol extinction below 14.5 km is noticeably affected by several eruptions of Redoubt Volcano (Alaska) in late March, which also injected ash into the stratosphere.

3.3. Magnitude and Upper Altitude of Aerosol Perturbation

[19] From here forward, the discussion does not relate to cloud detections and global background extinction. All northern hemispheric data are used together, unless indicated. In September 2008, NH median profiles of NIR extinction show a significant increase relative to each of the previous four Septembers (2004–2007; see Figure 4). The interannual variability in September between 2004 and 2007 is remarkably small. At the 9.5 km peak, extinction is ~8 times the September 2004–2007 median value (or 22 standard deviations above the median).

[20] The September 2008 data also show plenty of stratospheric aerosol extinction variability prior to fully dispersing over the Northern Hemisphere (Figure 3) with some profiles showing a very sharp peak at 17.5 km (e.g., Figure 5), with almost an order of magnitude greater extinction than the monthly median (Figure 4). Figure 5 also illustrates that both MAESTRO and NIR Imager observed a perturbed aerosol extinction profile up to 18.5 km at 57°N. The relative precision at the stratospheric peak is 6% and 1% for MAESTRO and NIR Imager on 1.4 and 1.0 km thick retrieval layers, respectively, providing confidence in the consistency of both ACE instruments. Below 18 km, the lack of agreement within error bars may be due to the differences in the size and shape of the field-of-views of the two instruments in the presence of a spatially inhomogeneous aerosol plume (on a horizontal scale of 20 km), with some contribution from offset tangent heights in the MAESTRO data. The latter source of error can be large for a sharply peaked profile. The MAESTRO retrieval appears to have a high bias in the middle stratosphere relative to NIR Imager.

[21] Figure 6 illustrates the median of several profiles from September 2008 which provide evidence from both aerosol-measuring instruments of a sharp peak at an altitude of 16.5 ± 1 km, above the peak altitude suggested in Figure 4 from median data. These observations are located at a variety of longitudes in both the eastern and western hemisphere, indicating that even after a month of dispersing horizontally, the vertical dispersion in the stratosphere occurs slowly. The MAESTRO volcanic aerosol extinction measurements support the validity of the NIR Imager extinction profiles, and vice versa.

3.4. Observed Properties of the Aerosol Layers: Thickness and Rates of Descent and Removal

[22] The lower, more optically thick aerosol layer shown in Figure 4 has a full width half maximum (FWHM) of ~2.5 km, spanning from ~8 to 10.5 km and vanishes by the end of November 2008 (Figure 7a). Figure 7b illustrates the time series of the extinction ratio (relative to Rayleigh extinction), which is a measure of the perturbation to extinction by aerosols. N_2O and HNO_3 as measured

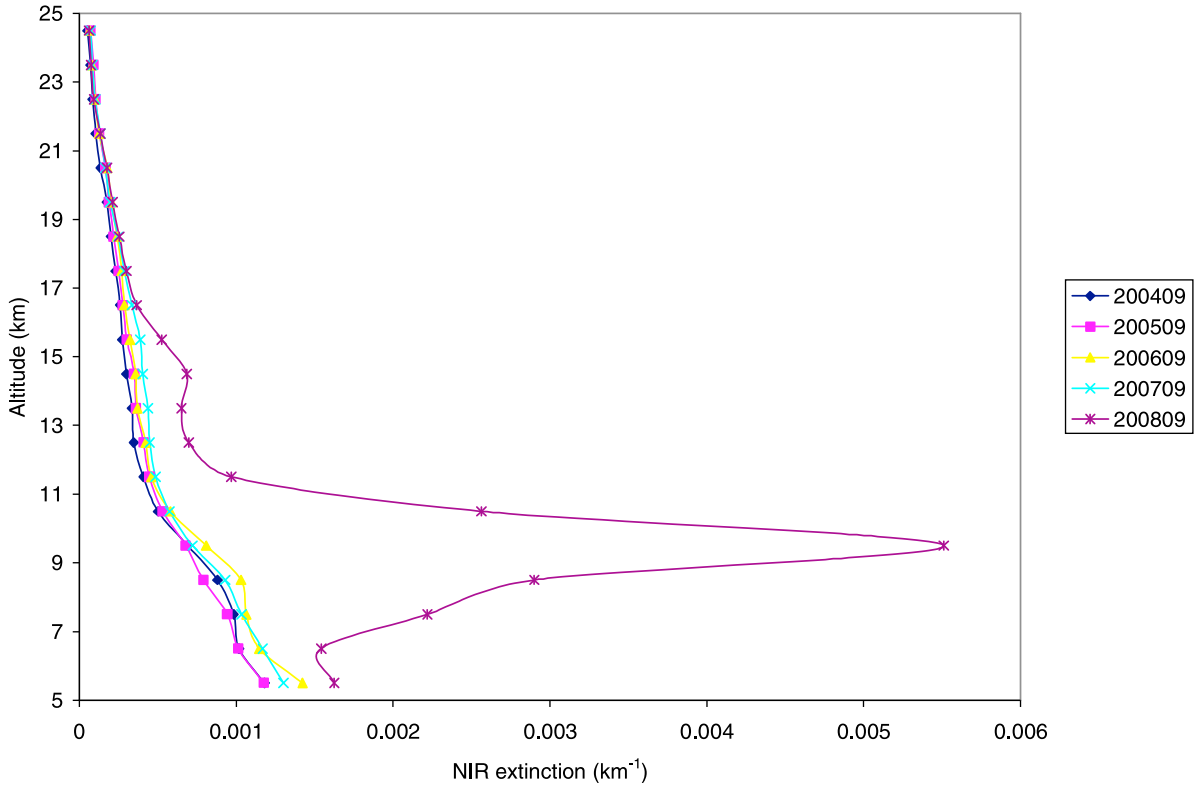

Figure 4. Northern Hemisphere median NIR extinction profiles for Septembers in 2004–2008.

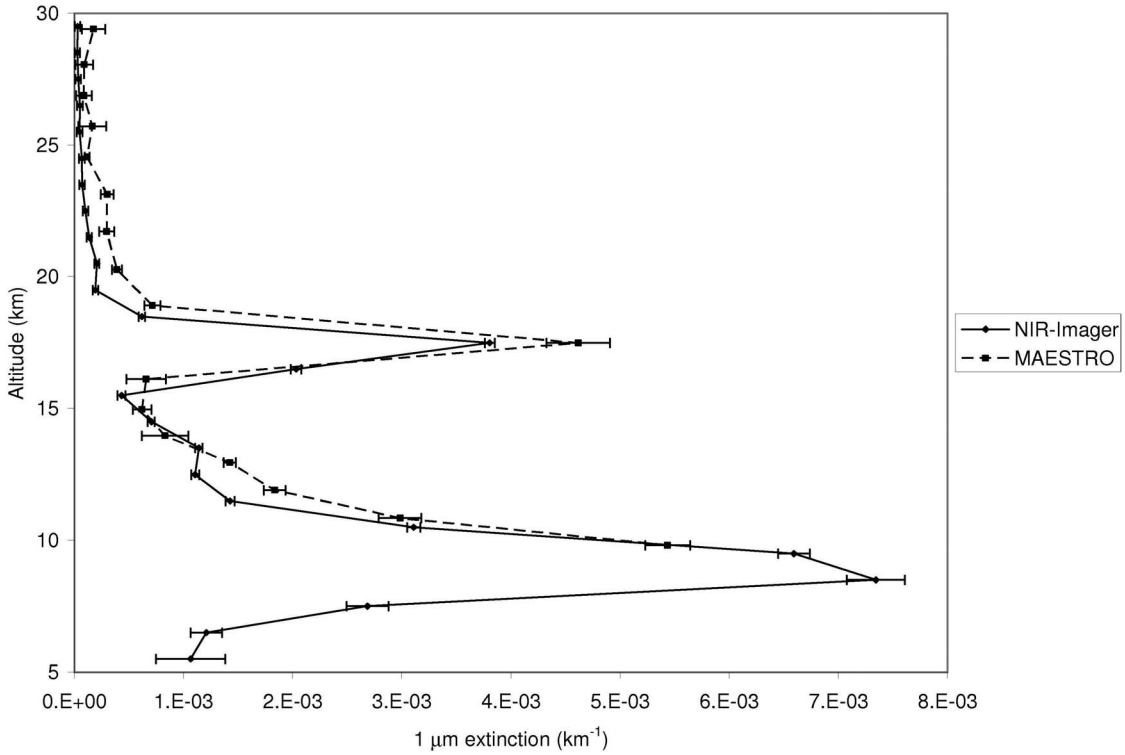

Figure 5. Sample NIR extinction profiles measured by MAESTRO and NIR Imager on 8 September 2008 at northern midlatitude (56.5°N, 35.1°W) far from Kasatochi Volcano, but showing clear evidence of a sharp layer in the lower stratosphere and a second layer peaking at 8.5 km near the midlatitude tropopause.

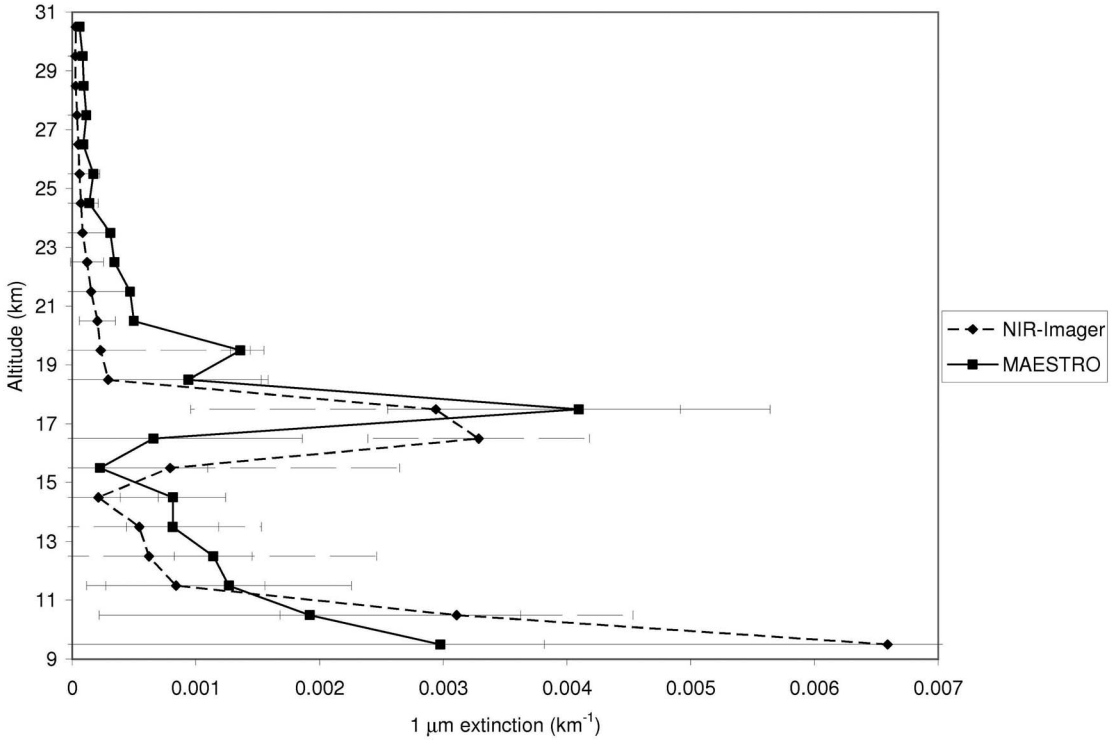

Figure 6. Comparison of median extinction profiles (N = 11) observed by NIR Imager and MAESTRO. All NIR Imager atmospheric extinction profiles peaking at 17.5, 16.5, or 15.5 km with peak extinction $>3 \times 10^{-3}$ km^{-1} were selected. The data covers the 4–18 September 2008 period and latitudes between 45.9° and 73.8°N. Data from both instruments are included in the altitude range where the NIR Imager extinction uncertainty is <100% (i.e., up to ~30 km). The horizontal bars are the standard deviation of the measurements at each altitude.

by FTS are used as tracers of the descent of air by large-scale subsidence at middle to high northern latitudes (discussed below). The peak of this lower layer is located below the thermal tropopause at all but the northernmost latitudes (see Figure 8a).

[23] In addition to this aerosol layer, there is a second layer that lies above the height of the extratropical tropopause, which is optically thinner with a NIR extinction peak at 14.5 km in September 2008, also seen by CALIPSO [*Yang et al.*, 2010]. This layer can be seen in October 2008, when latitudinal sampling of the Northern Hemisphere is sufficient to study the zonal median distribution in 15° latitude bands (Figure 8a). The upper layer peaks at 14.5 ± 1 km between 45 and 85°N, but at lower latitudes, the peak height reaches up to 18.5 km at low latitudes (15–30°N). This layer descends slowly through the end of 2008 and then accelerates to ~2 km/month from January to March 2009 as it enters the troposphere (Figure 7b). Note that the thermal tropopause in March 2009 is typically at 8.5 km according to analyses from the Canadian Meteorological Centre sampled at ACE measurement locations [*Boone et al.*, 2005] (which are limited to latitudes >50°N in this month). The peak altitude of the extinction ratio has descended from 13.5 km in December 2008 to 10.5, 8.5, and 7.5 km for January, February, and March 2009, respectively (Figure 7b). The NH latitudinal distribution is also shown for February 2009 in Figure 8b. As for October 2008 (Figure 8a), the median extinction at low northern latitudes (e.g., 15–30°N) is significantly lower than at middle and high latitudes for altitudes below 10.5 km, indicating a faster removal rate in the former. The layer at 8.5 km in Figure 8b, most evident in the 30–45°N band (and seen more clearly in the NH median extinction ratio; see Figure 7b) is the upper aerosol layer and has descended several kilometers from the lower stratosphere in October 2008 (Figure 8a) to the upper troposphere.

[24] The extinction in this upper layer does not simply decay with time as is seen in the lower aerosol layer. The extinction at the upper peak increases from September to October 2008, presumably as sulphate aerosols continue to grow in size. Also, between February 2009 and March 2009, a significant increase in extinction ratio is observed, likely due to continuing coagulation [*Pitts and Thomason*, 1993; *Pnueli et al.*, 1991; *Beeckmans*, 1965; *Debry and Sportisse*, 2007] and water uptake by the hygroscopic sulphate aerosols as the upper layer descends in the more humid troposphere. This increase is also confirmed by the monthly time series of optical depth in the 5.0–25.0 km partial column (Figure 9), which shows the increasing trend in February and March 2009.

[25] A possible explanation for the different removal rates of the two aerosol layers seen in Figure 7 is that the optically thick lower layer was composed of heavier particles than the optically thinner upper layer (see below). Also, the timing of

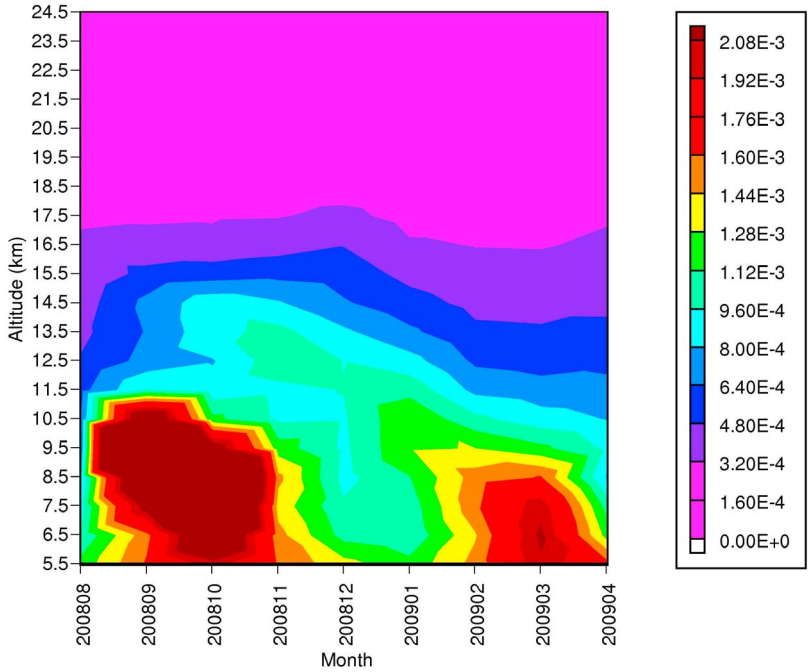

Figure 7a. Temporal evolution of the median atmospheric extinction in the Northern Hemisphere. August 2008 does not contain any observations of the Kasatochi plume (see section 3.1) and thus represents background atmospheric extinction.

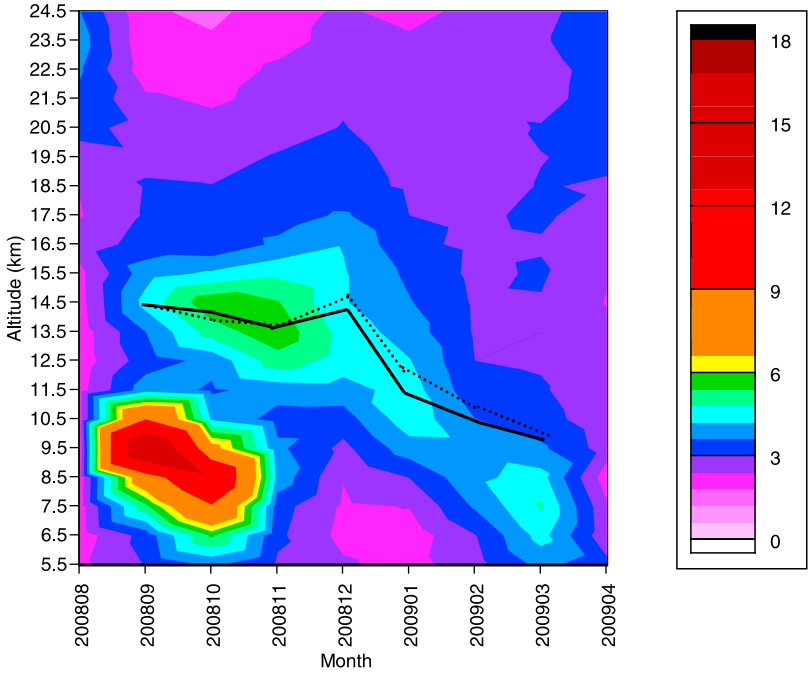

Figure 7b. Same as Figure 7a, but for extinction ratio. For each month in the period from August 2008 to April 2009, the NH median atmospheric extinction is normalized by the Rayleigh extinction as a function of altitude. The Rayleigh extinction is calculated for the monthly averaged latitude of the NIR Imager NH observations. The solid and dashed lines show the descent of the 293 ppbv isopleth of N_2O and the 211 ppbv isopleth of HNO_3, respectively, during the post-Kasatochi period and correspond to the altitude of the upper layer in September 2008.

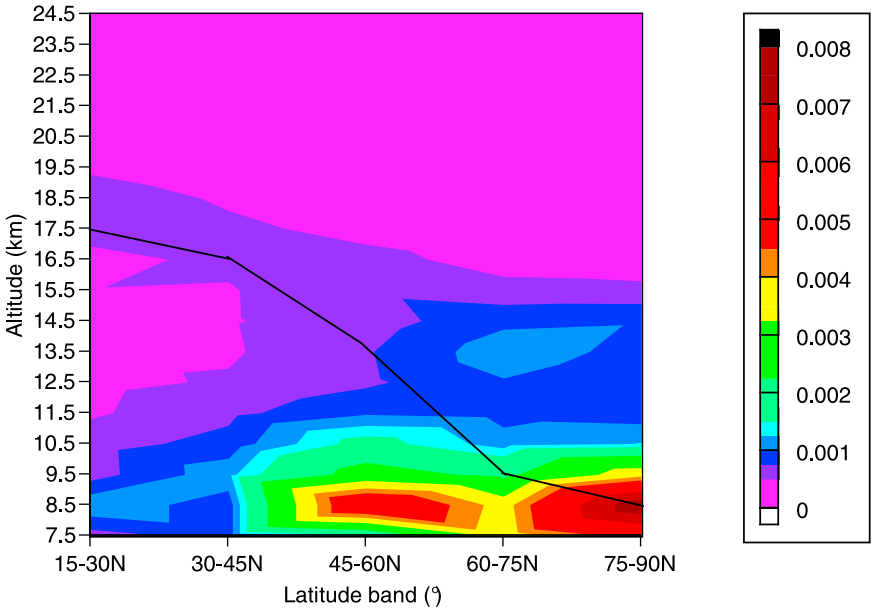

Figure 8a. Zonal median atmospheric extinction (km^{-1}) measured by NIR Imager at ~1020 nm in October 2008 as a function of latitude band. The median height of the thermal tropopause as sampled by ACE is shown by the black line.

the volcanic eruption may have been a factor since cumulonimbus clouds are more frequent and reach the tropopause more frequently in September relative to boreal winter months. Thus, the removal by rainout would be much slower for the upper layer than the lower aerosol layer.

3.5. Particle Size Information

[26] MAESTRO can provide height-resolved information on particle size via the widely used Ångström exponent. The Ångström exponent is inversely related to the particle size and is determined from the wavelength-dependence of the measured aerosol extinction. As SO_2 is converted to sulphuric acid and deposited on existing aerosol, the growing aerosol is expected to lead to a decrease in the Ångström exponent. Initially, these aerosols could be so small that they could be relatively transparent to near-infrared extinction measurements, so that an ongoing coagulation process could cause a slow reduction to the Ångström exponent. As the resulting aerosols eventually become larger, the Ångström exponent is expected to become significantly and rapidly smaller.

[27] Before comparing the temporal evolution of the Ångström exponent from MAESTRO with the extinction time series from NIR Imager, it is worth noting that the

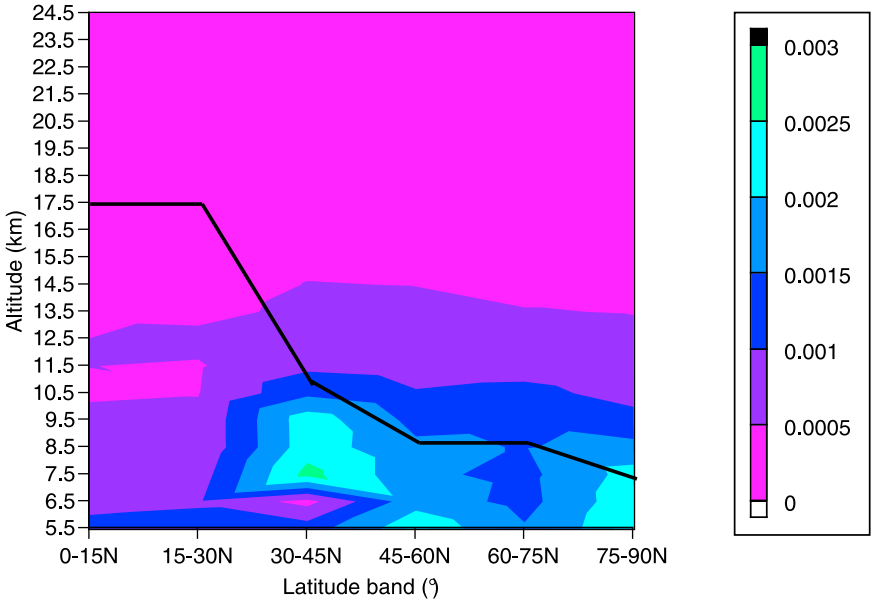

Figure 8b. Same as Figure 8a, but for February 2009.

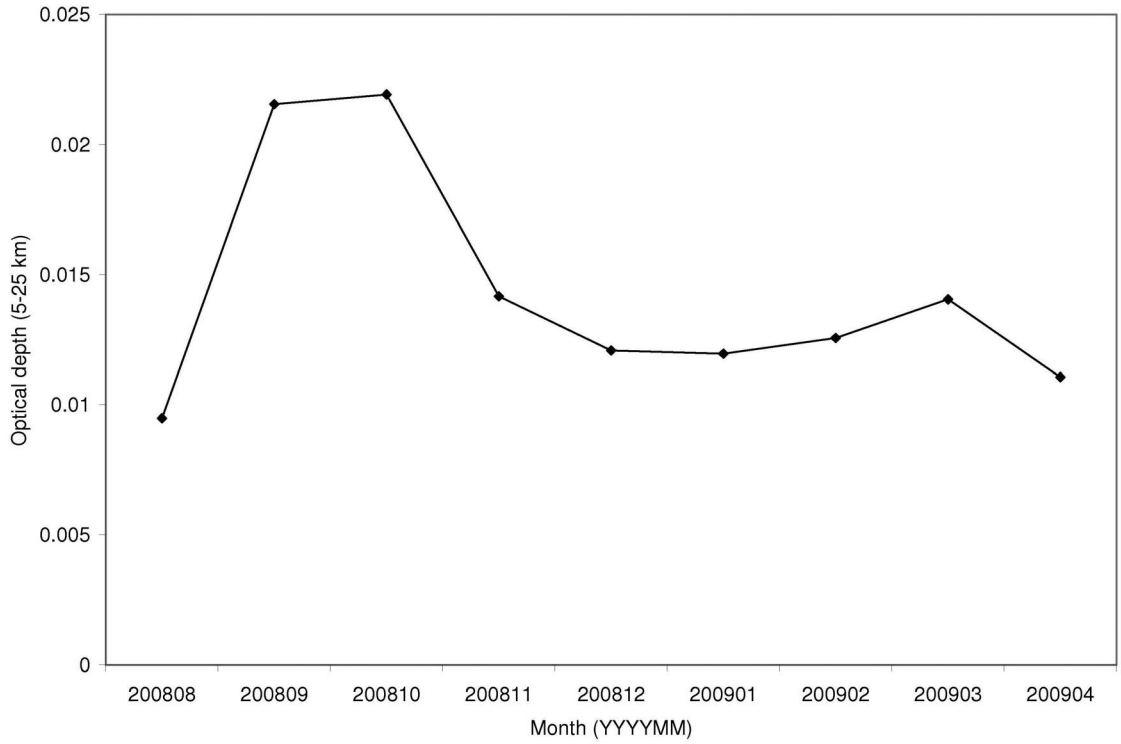

Figure 9. Time series of optical depth obtained by integrating the monthly median NH extinction from NIR Imager.

extinction time series at 779 and 1000 nm from MAESTRO are consistent with the NIR Imager observations illustrated in Figure 7a (not shown). Figure 10 illustrates that September 2008 has larger aerosol particles than the subsequent months (including March 2009 which is approaching background conditions), particularly at heights in between the two layers at ~10 and ~15 km composed partly of sulphate droplets. The larger particle size in between these layers is likely indicative

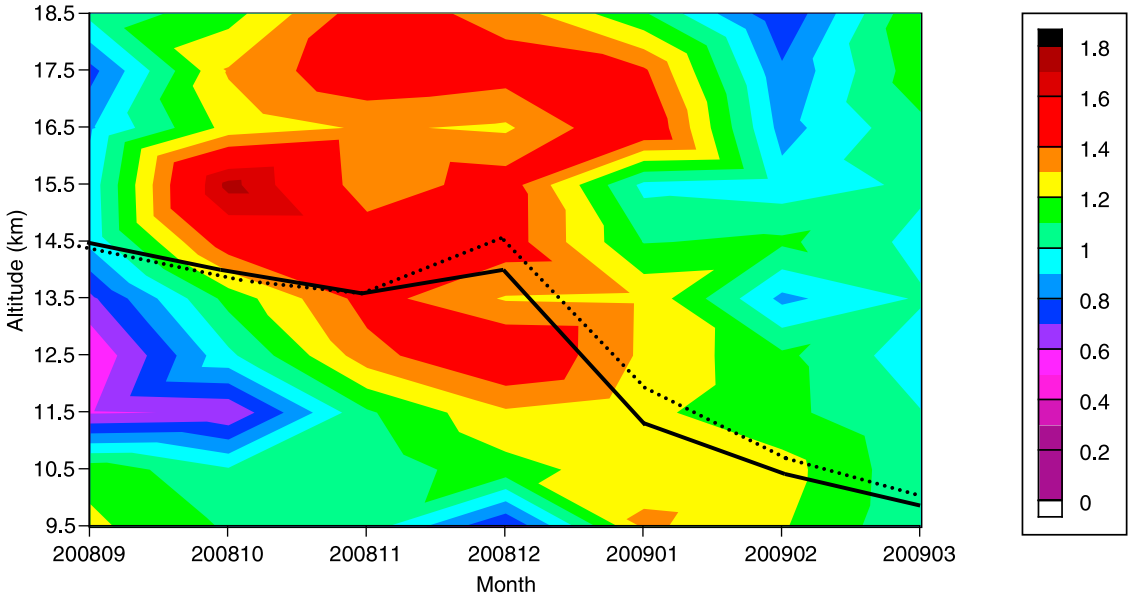

Figure 10. Aerosol Ångström exponent time series obtained from MAESTRO monthly median aerosol extinction vertical profiles at 779 and 1000 nm. The data are binned in 1 km vertical increments to compute the median profiles. The 293 ppbv isopleth of N_2O and the 211 ppbv isopleth of HNO_3 are shown as in Figure 7b to account for the variation in tropopause height with sampled latitude and to illustrate the large-scale subsidence of air starting from the September 2008 aerosol extinction peak height of 14.5 km.

of residual volcanic ash falling out from the upper layer. Volcanic ash persisted for more than a month following the Mount Hudson eruption [*Kerdiles and Diaz*, 1996], a high-latitude volcano of similar magnitude. Also, a stratospheric volcanic dust cloud was observed for at least three weeks following the eruption of El Chichón [*Robock and Matson*, 1983]. From Figure 10, it appears that smaller, sulphate aerosols are abundant in the lower layer (near 9.5 km) in September, where SO_2 also peaked [*Yang et al.*, 2010]. But, above this lower layer (11–18 km), the supply of SO_2 is more limited, and the sulphate aerosols take longer to grow and be detected by MAESTRO. Note also that the second smaller local maximum in the Ångström exponent profile for September 2008 is at ~15 km.

[28] At this altitude, in October 2008, an upper layer of smaller particles, presumably composed of sulphate aerosol, clearly emerges. This layer of smaller particles lies at the same height as the upper aerosol layer observed by NIR Imager (within ~1 km) and descends at the same rate. As this upper layer of smaller particles descends, its aerosol Ångström exponent steadily decreases, consistent with the notion that there is ongoing coagulation of sulphate aerosol [*Pitts and Thomason*, 1993] between September 2008 and March 2009, leading to particle growth and consequently more efficient scattering of radiation. In February and March 2009, the descent of the upper layer, visualized by the extinction ratio and Ångström exponent, has outpaced the descent of N_2O and HNO_3 (Figures 7b and 10, respectively). This may be due to gravitational sedimentation as particle size increases. A second factor could be that the peak of the extinction ratio is weighted to lower altitudes because of the sharply increasing gradient in water vapor with decreasing altitude. This would favor the hygroscopic growth and increasing extinction of the aerosols at the bottom of the layer.

[29] Assuming the aerosol is composed entirely of sulphate with particle sizes lognormally distributed, an effective radius (r_e) can be inferred from MAESTRO spectral extinctions. The effective variance was assumed to be 0.08 μm^2, appropriate for stratospheric aerosol [*Hansen and Travis*, 1974]. These r_e profiles may be biased high by the use of two longer wavelengths, reducing the sensitivity to fine aerosols. The inferred range of r_e is ~0.35 μm (at 15.5 km in October 2008) to ~0.6 μm (at 12.5 km in September 2008). A realistic change in the assumed effective variance did not affect the inferred r_e significantly for large (0.6 μm) effective radius.

4. Concluding Remarks

[30] Comparing the NH median of ACE-FTS temperature profiles in October 2008 to the previous four Octobers (2004–2007) reveals that temperature biases between these samples are not significant (not shown) between 12 and 15 km, where a relatively large increase in atmospheric extinction occurred. The FTS temperature retrieval [*Boone et al.*, 2005] is precise, with random errors of 2 K [*Sica et al.*, 2008] and a lower-altitude limit of ~12 km. Also, the profiles of ~33 trace gases retrieved from ACE-FTS observations in September 2008 do not exhibit significant differences from climatological values from ACE-FTS.

[31] In summary, two ACE instruments observed the Kasatochi volcanic plume spread over the Northern Hemisphere during September 2008. The more optically thick upper tropospheric component vanishes after less than four months whereas the upper maximum persists into March 2009, broadening in height and descending with time, raising background aerosol levels in the Northern Hemisphere upper troposphere and lower stratosphere.

[32] **Acknowledgments.** The ACE mission is supported primarily by the Canadian Space Agency. Some support was also provided by the UK Natural Environment Research Council.

References

Beeckmans, J. M. (1965), Numerical solutions of Smoluchowski's equations for the coagulation of uncharged aerosols, *Can. J. Chem.*, *43*, 2312–2318, doi:10.1139/v65-312.

Bernath, P. (2006), Atmospheric Chemistry Experiment (ACE): Analytical chemistry from orbit, *Trends Analyt. Chem.*, *25*, 647–654, doi:10.1016/j.trac.2006.05.001.

Bogumil, K., et al. (2003), Measurements of molecular absorption spectra with the SCIAMACHY pre-flight model: Instrument characterization and reference data for atmospheric remote-sensing in the 230–2380 nm region, *J. Photochem. Photobiol. A*, *157*, 167–184, doi:10.1016/S1010-6030(03)00062-5.

Boone, C. D., R. Nassar, K. A. Walker, Y. Rochon, S. D. McLeod, C. P. Rinsland, and P. F. Bernath (2005), Retrievals for the atmospheric chemistry experiment Fourier transform spectrometer, *Appl. Opt.*, *44*, 7218–7231, doi:10.1364/AO.44.007218.

Carn, S. A., N. A. Krotkov, V. Fioletov, K. Yang, A. J. Krueger, and D. Tarasick (2008), Emission, transport and validation of sulfur dioxide in the 2008 Okmok and Kasatochi eruption clouds, *Eos Trans. AGU*, *89* (53), Fall Meet. Suppl., Abstract A51J–07.

Chahine, M. T. (1970), Inverse problems in radiative transfer: Determination of atmospheric parameters, *J. Atmos. Sci.*, *27*, 960–967, doi:10.1175/1520-0469(1970)027<0960:IPIRTD>2.0.CO;2.

Debry, E., and B. Sportisse (2007), Solving aerosol coagulation with size-binning methods, *Appl. Numer. Math.*, *57*, 1008–1020, doi:10.1016/j.apnum.2006.09.007.

Dodion, J., et al. (2007), Cloud detection in the upper troposphere-lower stratosphere region via ACE imagers: A qualitative study, *J. Geophys. Res.*, *112*, D03208, doi:10.1029/2006JD007160.

Dutton, E. G., and J. R. Christy (1992), Solar radiative forcing at selected locations and evidence for global lower tropospheric cooling following the eruptions of El Chichón and Pinatubo, *Geophys. Res. Lett.*, *19*, 2313–2316, doi:10.1029/92GL02495.

Fromm, M., J. Alfred, and M. Pitts (2003), A unified long-term, high-latitude stratospheric aerosol and cloud database using SAM II, SAGE II, and POAM II/III data: Algorithm description, database definition, and climatology, *J. Geophys. Res.*, *108*(D12), 4366, doi:10.1029/2002JD002772.

Gilbert, K. L., D. N. Turnbull, K. A. Walker, C. D. Boone, S. D. McLeod, M. Butler, R. Skelton, P. F. Bernath, F. Chateauneuf, and M.-A. Soucy (2007), The onboard imagers for the Canadian ACE SCISAT-1 mission, *J. Geophys. Res.*, *112*, D12207, doi:10.1029/2006JD007714.

Hansen, J. E., and L. D. Travis (1974), Light scattering in planetary atmospheres, *Space Sci. Rev.*, *16*, 527–610, doi:10.1007/BF00168069.

Kerdiles, H., and R. Diaz (1996), Mapping of volcanic ashes from the 1991 Hudson eruption using NOAA-AVHRR data, *Int. J. Remote Sens.*, *17*, 1981–1995, doi:10.1080/01431169608948754.

Larsen, J., C. Neal, P. Webley, J. Freymueller, M. Haney, S. McNutt, D. Schneider, S. Prejean, J. Schaefer, and R. Wessels (2009), Eruption of Alaska Volcano Breaks Historic Pattern, *Eos Trans. AGU*, *90*(20), doi:10.1029/2009EO200001.

McElroy, C. T., et al. (2007), The ACE-MAESTRO instrument on SCISAT: Description, performance, and preliminary results, *Appl. Opt.*, *46*, 4341–4356, doi:10.1364/AO.46.004341.

McLinden, C. A., C. S. Haley, and C. E. Sioris (2006), Diurnal effects in limb scatter observations, *J. Geophys. Res.*, *111*, D14302, doi:10.1029/2005JD006628.

Pitts, M. C., and L. W. Thomason (1993), The impact of the eruptions of Mount Pinatubo and Cerro Hudson on Antarctic aerosol levels during the 1991 austral spring, *Geophys. Res. Lett.*, *20*, 2451–2454, doi:10.1029/93GL02160.

Pnueli, D., C. Gutfinger, and M. Fichman (1991), A turbulent-Brownian model for aerosol coagulation, *Aerosol Sci. Technol.*, *14*, 201–209, doi:10.1080/02786829108959483.

Rix, M., et al. (2009), Satellite monitoring of volcanic sulfur dioxide emissions for early warning of volcanic hazards, *IEEE J. Selec. Top. Appl. Earth Observ. Remote Sens.*, *2*, 196–206, doi:10.1109/JSTARS.2009.2031120.

Robock, A., and M. Matson (1983), Circumglobal transport of the El Chichón volcanic dust cloud, *Science*, *221*, 195–197, doi:10.1126/science.221.4606.195.

Salby, M. L. (1996), *Fundamentals of Atmospheric Physics*, Academic, San Diego, Calif.

Sica, R. J., et al. (2008), Validation of the Atmospheric Chemistry Experiment (ACE) version 2.2 temperature using ground-based and space-borne measurements, *Atmos. Chem. Phys.*, *8*, 35–62, doi:10.5194/acp-8-35-2008.

Theys, N., M. Van Roozendael, B. Dils, F. Hendrick, N. Hao, and M. De Mazière (2009), First satellite detection of volcanic bromine monoxide emission after the Kasatochi eruption, *Geophys. Res. Lett.*, *36*, L03809, doi:10.1029/2008GL036552.

Vanhellemont, F., et al. (2005), A first comparison of GOMOS aerosol extinction retrievals with other measurements, *Adv. Space Res.*, *36*, 894–898, doi:10.1016/j.asr.2005.04.094.

Vanhellemont, F., et al. (2008), Aerosol extinction profiles at 525 nm and 1020 nm derived from ACE imager data: Comparisons with GOMOS, SAGE II, SAGE III, POAM III, and OSIRIS, *Atmos. Chem. Phys.*, *8*, 2027–2037, doi:10.5194/acp-8-2027-2008.

Yang, K., X. Liu, P. K. Bhartia, N. A. Krotkov, S. A. Carn, E. J. Hughes, A. J. Krueger, R. J. D. Spurr, and S. G. Trahan (2010), Direct retrieval of sulfur dioxide amount and altitude from spaceborne hyperspectral UV measurements: Theory and application, *J. Geophys. Res.*, *115*, D00L09, doi:10.1029/2010JD013982.

P. F. Bernath, Department of Chemistry, University of York, Heslington, York YO10 5DD, UK.

C. D. Boone, Department of Chemistry, University of Waterloo, Waterloo, ON, Canada N2L 3G1.

C. T. McElroy, C. A. McLinden, and C. E. Sioris, Environment Canada, 4905 Dufferin St., Toronto, ON, Canada M3H 5T4. (csioris@cfa.harvard.edu)

J. Zou, Department of Physics, University of Toronto, 60 St. George St., Toronto, ON, Canada M5S 1A7.